Journal of Physics: Condensed Matter

Magnetic structure in iron borates $RFe_3(BO_3)_4$(R = Y,Ho): a neutron diffraction and magnetization study

To cite this article: C Ritter *et al* 2008 *J. Phys.: Condens. Matter* **20** 365209

J. Phys.: Condens. Matter **20** (2008) 365209 (9pp) doi:10.1088/0953-8984/20/36/365209

Magnetic structure in iron borates $RFe_3(BO_3)_4$(R = Y, Ho): a neutron diffraction and magnetization study

C Ritter[1], A Vorotynov[2], A Pankrats[2], G Petrakovskiĭ[2], V Temerov[2], I Gudim[2] and R Szymczak[3]

[1] Institute Laue-Langevin, Boite Postale 156, F-38042 Grenoble, France
[2] L V Kirenskiĭ Institute of Physics, Siberian Branch of RAS, Krasnoyarsk 660036, Russia
[3] Institute of Physics, Polish Academy of Sciences, PL-02668 Warsaw, Poland

E-mail: ritter@ill.fr

Received 21 April 2008, in final form 18 July 2008
Published 14 August 2008
Online at stacks.iop.org/JPhysCM/20/365209

Abstract

Neutron diffraction, susceptibility and magnetization measurements were performed on iron borates $RFe_3(BO_3)_4$ (R = Y, Ho) to investigate the low temperature magnetic structures and to clarify the role of the rare earth in the formation of the long-range magnetic order. Both compounds see an identical magnetic propagation vector $\tau = [0, 0, 1/2]$ within the $P3_121$ crystallographic space group appear at Néel temperatures of $T_N = 37$ K for the Y and $T_N = 38$ K for the Ho compound. The strong polarization effect of the Fe sublattice on the Ho^{3+} ions leads to the simultaneous ordering of both sublattices while the competition between their anisotropies governs the spin-reorientation process at $T_{SR} = 5$ K. The results obtained are discussed in the framework of the determined structural details and the specific rare-earth ions present including information on compounds investigated earlier.

(Some figures in this article are in colour only in the electronic version)

1. Introduction

Rare-earth ferroborates with the general formula $RFe_3(BO_3)_4$ (where R is a rare earth or Y ion) have recently attracted considerable interest due to their promising magnetoelectrical properties, which suggest that these compounds belong to the family of multiferroics whose investigation has recently become a topic of broad interest [1–5].

The crystal structure of these borates is derived from the structure of the mineral huntite [6, 7]. The good optoelectronic properties found for the Al-containing borates $RAl_3(BO_3)_4$ are related to the absence of an inversion centre in the crystallographic space group $R32$ typical for these compounds. A transition from $R32$ to $P3_121$ takes place in the ferroborates at a transition temperature which depends directly on the rare-earth ionic size [8, 9]. A transition to a magnetically long-range ordered state can be found at a temperature which again is directly related to the ionic size of R. The presence of two possible magnetic sublattices formed by the rare earth and the iron ions leads to a complicated magnetic behaviour which is strongly influenced by the different magnetic interactions and pathways. An interesting aspect of the structure is its strong structural anisotropy which is caused by the Fe sublattice forming helicoidal chains of Fe^{3+} ions along the c axis. The distance between Fe^{3+} ions along these chains is significantly shorter than the distance between neighbouring chains and leads to some kind of one-dimensional structural element. At the same time the rare-earth ions are well isolated from each other located in trigonal prisms RO_6 with no direct R–O–R links. A detailed description and a picture of the structure can be found in Campa *et al* [7]. The combination of a strongly anisotropic crystal structure with the presence of highly anisotropic magnetic rare-earth ions characterizes these compounds and it was suspected to be at the origin of a magnetic behaviour dominated by polarization and spin-reorientation phenomena. Magnetic measurements, mostly on the Gd and Nd compounds, were interpreted in these terms but direct information on the magnetic structures in rare-earth ferroborates using microscopic methods is, however, still scarce.

In our previous paper [10] we have determined the nuclear and magnetic structure of $TbFe_3(BO_3)_4$. A structural phase transition from $R32$ to $P3_121$ takes place at $T = 192$ K. An antiferromagnetic coupling along the helicoidal chains of Fe atoms with a magnetic propagation vector $\tau = [0, 0, 1/2]$ sets in at about 40 K. Our study confirmed the polarization effect of the long-range-ordered Fe sublattice on the Tb spins. A similar behaviour with both sublattices ordering simultaneously was found by Fischer *et al* [11] in $NdFe_3(BO_3)_4$, the only other ferroborate where the magnetic structure had been studied with neutron diffraction. Although both compounds see an identical propagation vector $\tau = [0, 0, 1/2]$ (describing the structure in $P3_121$), the spin directions are very different. While in the Tb compound Tb and Fe spins are nearly exclusively oriented along the c direction, the Nd compound sees spins of both sublattices confined to the a–b plane, indicating the strong role played by the anisotropy of the rare-earth ion present. In order to clarify further the role played by the rare-earth anisotropy and sublattice, the interatomic bond distances and exchange pathways we performed studies on the related compounds $YFe_3(BO_3)_4$ and $HoFe_3(BO_3)_4$. While the Y compound should allow us to study the magnetic behaviour of the iron sublattice in the absence of the influence of a strong rare-earth sublattice the Ho compound should open up the possibility to study the differences induced by the rare-earth magnetic anisotropy. Spectroscopic data on the Ho compound have recently been performed and an in-plane magnetic structure stabilized by the easy-plane magnetic anisotropy of the rare-earth sublattice has been proposed [12]. From the work of Hinatsu *et al* [9] it is known that both compounds see a magnetic transition at about 40 K and a structural transition from $P3_121$ to $R32$ at about 440 K.

2. Experimental details

2.1. Sample preparation

$HoFe_3(^{11}BO_3)_4$ and $YFe_3(^{11}BO_3)_4$ single crystals were grown from a bismuth trimolybdate solution-melt with a nonstoichiometric composition of the crystal constitutive oxides of 75 mass% $(Bi_2Mo_3O_{12} + 3\,^{11}B_2O_3 + 0.5Ho_2O_3) + 25$ mass% $HoFe_3(^{11}BO_3)_4$ and 77 mass% $(Bi_2Mo_3O_{12} + 3\,^{11}B_2O_3 + 0.5Y_2O_3) + 23$ mass% $YFe_3(^{11}BO_3)_4$ with saturation temperatures of $T_{sat} \approx 960\,^{\circ}C$ and $940\,^{\circ}C$, respectively. In these solution melts the trigonal $HoFe_3(^{11}BO_3)_4$ and $YFe_3(^{11}BO_3)_4$ are the high temperature phases and crystallize at least up to $T \approx 900\,^{\circ}C$. The solution-melts with a mass of 100 g were prepared in a platinum crucible. They were kept for 8–10 h at $T = 1100\,^{\circ}C$ for homogenization with permanent mixing by a reversibly rotating platinum rod. Then the temperature was lowered to $T = T_{sat} - (5–7)\,^{\circ}C$ and the rod was taken up to the furnace orifice. The spontaneous crystallization takes place inside the thin overcooled layer of the solution-melt which stays on the rod. The rod was again settled down into the solution-melt and the temperature was lowered by $(3–6)\,^{\circ}C/24$ h. The crystallization process was stopped at $T = 900–905\,^{\circ}C$. Crystals with linear dimensions up to 7 mm were grown. Powders for the neutron measurements were prepared from these crystals by grinding.

2.2. Magnetization and neutron diffraction measurements

Neutron diffraction data were taken at the Institut Laue-Langevin in Grenoble, France, using the high resolution powder diffractometer D1A ($\lambda = 1.91$ Å) and the high flux powder diffractometer D1B ($\lambda = 2.52$ Å). The temperature dependence of the neutron diffraction pattern of $YFe_3(BO_3)_4$ was measured on D1B with a temperature resolution of about 1 K taking a spectrum every 10 min. High resolution data were taken at 2 and 50 K and at room temperature, while an additional dataset was collected at 520 K using $\lambda = 1.39$ Å. The Ho compound was exclusively studied on D1A: between 2 and 44 K spectra were taken every degree in order to study in detail the magnetic phase transition. Data just above T_N at 50 K and at room temperature were again complemented with a dataset using $\lambda = 1.39$ Å at 520 K in the region where the compound should show the hexagonal structure type.

Magnetization and susceptibility measurements were studied on single crystals of $HoFe_3(BO_3)_4$ at temperatures 2–300 K in magnetic fields up to 5 T using the SQUID magnetometer MPMS-5 at the Institute of Physics PAS in Warsaw.

3. Results and discussion

The crystallographic structure of both compounds within the paramagnetic state was verified using the high resolution data taken at 520 K, at room temperature and at 50 K. As expected it can be described within the space group $R32$ at 520 K. The Rietveld refinement using the program FULLPROF [13] ascertained the space group $P3_121$ to be the correct space group at room temperature and below. Details of the refined results are shown in tables 1 and 2. Both compounds are free from impurities.

Comparing the interatomic distances and angles of both compounds given in tables 1 and 2 one can state a nearly identical structure. A differing magnetic behaviour at lower temperatures (see below) can therefore not be connected to structural differences present in the paramagnetic state but have to be exclusively related to the different rare-earth ion present. Figure 1 shows the low temperature thermal dependence of the neutron diffraction pattern (thermodiffractogram) of $YFe_3(BO_3)_4$. Additional Bragg peaks of magnetic origin appear at about 35 K. A fit of the integrated intensity of the strongest magnetic peaks as a function of temperature (not shown here) indicates that the development of these additional peaks is continuous. There is no sign of a spin-reorientation process. The magnetic peaks can be indexed with a magnetic propagation vector of $\tau = [0\ 0\ 1/2]$, corresponding to a magnetic unit cell doubled in the hexagonal c direction.

The high resolution data measured at 2 K were successfully refined (figure 2) using a model for the magnetic structure which sees the Fe spins antiferromagnetically coupled in the c direction while being ferromagnetically coupled within the a–b basal plane. Figure 3 displays the arrangement of the magnetic spins. Due to the trigonal structure of the compound it is not possible to determine the spin direction within the basal plane from powder diffraction

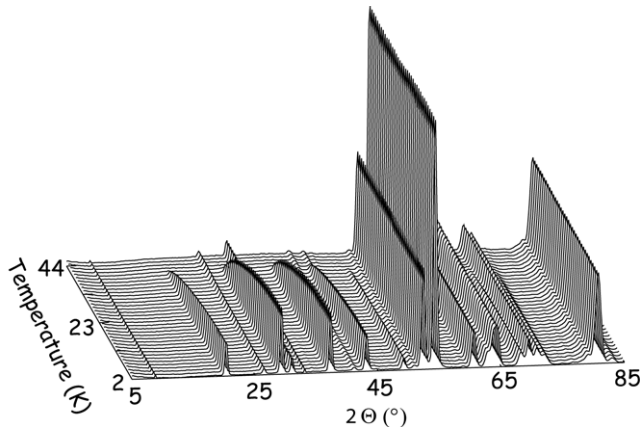

Figure 1. Thermal dependence of the neutron diffraction pattern of $YFe_3(BO_3)_4$ ($\lambda = 2.52$ Å).

Table 1. Lattice constants, atomic coordinates in $R32$, interatomic distances and angles for $YFe_3(BO_3)_4$ and $HoFe_3(BO_3)_4$ at 520 K.

520 K	Y	Ho
a (Å)	9.5428(5)	9.5337(1)
c (Å)	7.5818(4)	7.5711(1)
RE (3a) x	0	0
y	0	0
z	0	0
Fe (9d) x	0.5493(1)	0.5492(1)
y	0	0
z	0	0
O1 (9e) x	0.8563(2)	0.8554(2)
y	0	0
z	1/2	1/2
O2 (9e) x	0.5922(2)	0.5926(2)
y	0	0
z	1/2	1/2
O3 (18f) x	0.0250(1)	0.0247(1)
y	0.2113(1)	0.2111(1)
z	0.1815(2)	0.1825(2)
B1 (3b) x	0	0
y	0	0
z	1/2	1/2
B2 (9e) x	0.4485(1)	0.4481(2)
y	0	0
z	1/2	1/2
6 × RE–O3 (Å)	2.353(1)	2.354(1)
2 × Fe–O1 (Å)	2.025(1)	2.017(2)
2 × Fe–O2 (Å)	2.038(1)	2.033(2)
2 × Fe–O3 (Å)	1.970(1)	1.965(1)
Fe–Fe (Å)	3.1864(6)	3.1824(7)
Fe–O1–Fe (deg)	103.8(1)	104.2(1)
Fe–O2–Fe (deg)	102.9(1)	103.0(1)
Tb–O3–Fe (deg)	121.1(1)	121.0(1)

data as the magnetic reflections containing the requested information appear at identical 2Θ values.

The magnetic moment values of the two different crystallographic Fe sites within $P3_121$ amount to 4.18(25) μ_B for the Fe1 site and 3.83(13) μ_B for the Fe2 site. As they are equal within the error bars we have to accept that they cannot be differentiated, so the final refinement was done with a coupled magnetic moment value amounting to 3.95(5) μ_B.

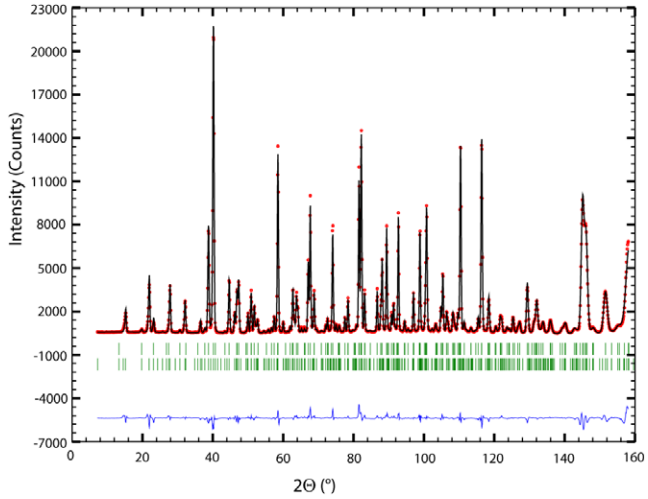

Figure 2. Observed (dots, red), calculated (line, black) and difference pattern of $YFe_3(BO_3)_4$ at 2 K refined in $P3_121$. The tick marks indicate the calculated position of the nuclear (upper row) and magnetic (lower row) Bragg peaks.

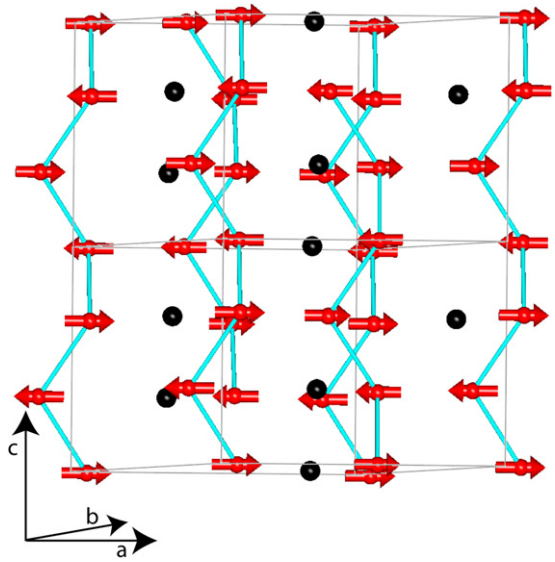

Figure 3. Magnetic structure of $YFe_3(BO_3)_4$. Fe spins in red (grey), while the direct Fe–Fe exchange along the helicoidal chains is indicated by blue (light grey) lines. The position of the Y atoms is indicated by black spheres.

Fixing the atomic coordinates to the values found from the refinement of the high resolution data at 2 K the temperature dependence of the magnetic moment was refined using the D1B data (figure 4). The solid line in figure 4 represents a fit of the data to a Brillouin function with $S = 5/2$.

In spite of the presence of the strong one-dimensional structure element which exists in these compounds (helicoidal chains of iron sites along the c axis (see figure 3)) the establishment of a normal 3D-type magnetic behaviour does not seem to be hindered. The interchain exchange interactions between Fe spins leading to this 3D ordered magnetic structure could either be transmitted through 16 Fe–O–O–Fe superexchange pathways as detailed in [10] or through Fe–O–B–O–Fe superexchange pathways.

Table 2. Lattice constants, atomic coordinates in $P3_121$ for $YFe_3(BO_3)_4$ and $HoFe_3(BO_3)_4$ at 2, 50 and 295 K.

		Y			Ho		
		2 K	50 K	295 K	2 K	50 K	295 K
a (Å)		9.517 21(9)	9.518 31(9)	9.525 06(8)	9.514 32(5)	9.523 65(5)	9.530 67(5)
c (Å)		7.545 29(10)	7.544 57(11)	7.555 80(10)	7.539 33(9)	7.544 36(7)	7.555 27(6)
RE (3a)	*x*	0.6654(8)	0.6650(8)	0.6651(8)	0.6644(10)	0.6657(5)	0.6665(6)
	y	0.6654(8)	0.6650(8)	0.6651(8)	0.6644(10)	0.6657(5)	0.6665(6)
Fe1 (3a)	*x*	0.1148(6)	0.1148(6)	0.1156(6)	0.1162(8)	0.1154(4)	0.1160(5)
	y	0.1148(6)	0.1148(6)	0.1156(6)	0.1162(8)	0.1154(4)	0.1160(5)
Fe2 (6c)	*x*	0.7886(5)	0.7883(5)	0.7864(5)	0.7873(6)	0.7883(3)	0.7868(3)
	y	0.4518(4)	0.4515(4)	0.4516(4)	0.4496(6)	0.4510(3)	0.4511(3)
	z	0.3447(5)	0.3443(5)	0.3416(5)	0.3453(5)	0.3448(3)	0.3422(3)
O1 (3b)	*y*	0.9205(9)	0.9215(8)	0.9204(9)	0.925(1)	0.9225(6)	0.9217(7)
O2 (6c)	*x*	0.4134(7)	0.4139(7)	0.4132(7)	0.419(1)	0.4171(5)	0.4157(6)
	y	0.7156(7)	0.7167(6)	0.7196(6)	0.722(1)	0.7206(5)	0.7235(5)
	z	0.1241(6)	0.1238(6)	0.1314(6)	0.1250(8)	0.1243(4)	0.1319(4)
O3 (6c)	*x*	0.8756(8)	0.8756(7)	0.8750(8)	0.873(1)	0.8763(5)	0.8752(6)
	y	0.6971(9)	0.6968(9)	0.695(1)	0.694(1)	0.6949(7)	0.6931(8)
	z	0.823(1)	0.823(1)	0.823(1)	0.823(1)	0.8231(7)	0.8228(8)
O4 (6c)	*x*	0.8553(9)	0.8557(8)	0.8566(8)	0.857(1)	0.8549(6)	0.8565(7)
	y	0.6401(9)	0.6393(9)	0.6398(9)	0.639(1)	0.6388(6)	0.6395(7)
	z	0.187(1)	0.187(1)	0.186(1)	0.189(1)	0.1854(7)	0.1864(8)
O5 (6c)	*x*	0.4784(7)	0.4784(7)	0.4784(6)	0.475(1)	0.4768(5)	0.4771(5)
	y	0.150(1)	0.1497(9)	0.1496(9)	0.144(1)	0.1454(7)	0.1453(8)
	z	0.843(1)	0.844(1)	0.842(1)	0.841 (1)	0.8421(8)	0.8401(9)
O6 (3b)	*x*	0.188(1)	0.188(1)	0.189(1)	0.184(1)	0.1851(8)	0.1853(9)
O7 (6c)	*x*	0.4774(7)	0.4781(7)	0.4797(7)	0.4752(9)	0.4770(5)	0.4788(5)
	y	0.4669(8)	0.4669(8)	0.4644(8)	0.464(1)	0.4659(5)	0.4640(7)
	z	0.8131(9)	0.8127(9)	0.8133(9)	0.816(1)	0.8128(6)	0.8138(7)
B1 (3b)	*x*	0.333(1)	0.332(1)	0.334(1)	0.329(2)	0.3318(8)	0.3324(9)
B2 (6c)	*x*	0.5528(9)	0.5526(9)	0.5538(9)	0.549(1)	0.5517(6)	0.5521(7)
	y	0.8758(7)	0.8756(6)	0.8790(7)	0.8774(8)	0.8763(4)	0.8791(5)
	z	0.1509(8)	0.1510(8)	0.1535(9)	0.149(1)	0.1504(5)	0.1543(6)
B3 (3b)	*y*	0.780(1)	0.780(1)	0.781(1)	0.779(1)	0.7795(8)	0.780(1)

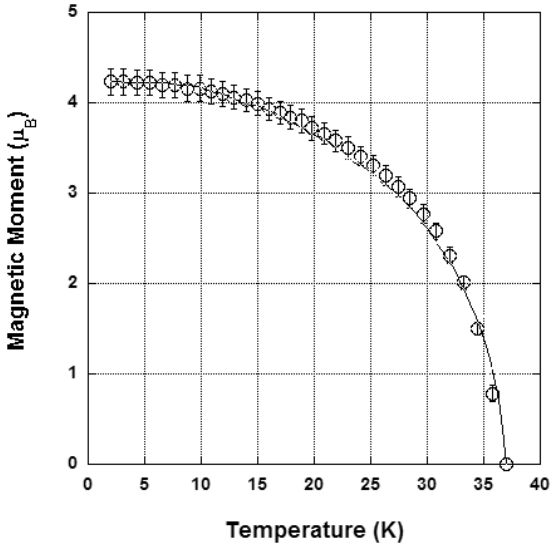

Figure 4. Temperature dependence of the magnetic moment value of Fe in $YFe_3(BO_3)_4$. The curve represents a fit of the data with a Brillouin function using $J = 5/2$.

The strength of the exchange via the first pathway should be rather weak while the exchange interaction via the BO_3 complex could have a strong exchange value as the boron and its surrounding oxygen ions form a strongly covalent hybridized complex. The overlapping of the electron density between the three participating oxygen atoms with each other in the complex is only negligible while simultaneously there exists a strong overlapping with the central boron atom. As a consequence the electron density is sufficient for a possible transfer via Fe–O–B–O–Fe superexchange pathway.

Due to the non-magnetic nature of the rare-earth ion a contribution to the three-dimensional ordering coming from exchange pathways including the Y sublattice can be excluded. The easy-plane magnetic structure of $YFe_3(BO_4)_3$ was recently confirmed by antiferromagnetic resonance measurements [14].

The low angle part of the thermodiffractogram of $HoFe_3(BO_3)_4$ is shown in figure 5. Contrary to the case of the Y compound the presence of additional Bragg peaks of magnetic origin is a two-step process. First, at about 38 K, magnetic peaks similar to the ones found in $YFe_3(BO_4)_3$ appear, before at about 5 K a strong change of peak intensities and the presence of new peaks takes place. This second magnetic ordering resembles strongly the one already found for the corresponding Tb compound. The magnetic propagation vector which indexes all magnetic Bragg peaks is again $\tau = [0\ 0\ 1/2]$ and is preserved when going through the transition at 5 K. This indicates that the change at 5 K is connected to the presence of a spin-reorientation process. Using the model for

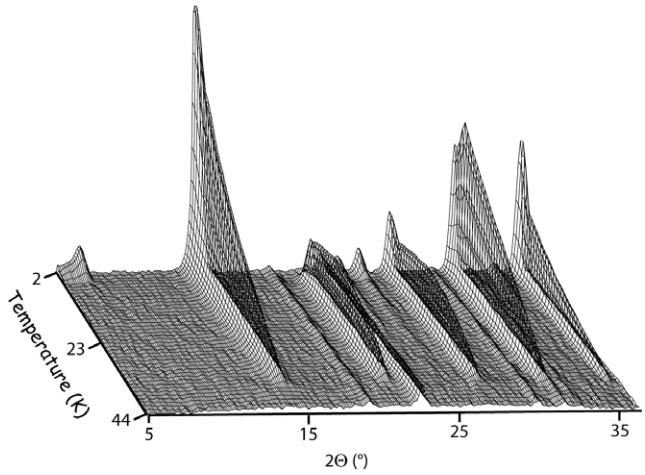

Figure 5. Thermal dependence of the neutron diffraction pattern of $HoFe_3(BO_3)_4$ ($\lambda = 1.91$ Å).

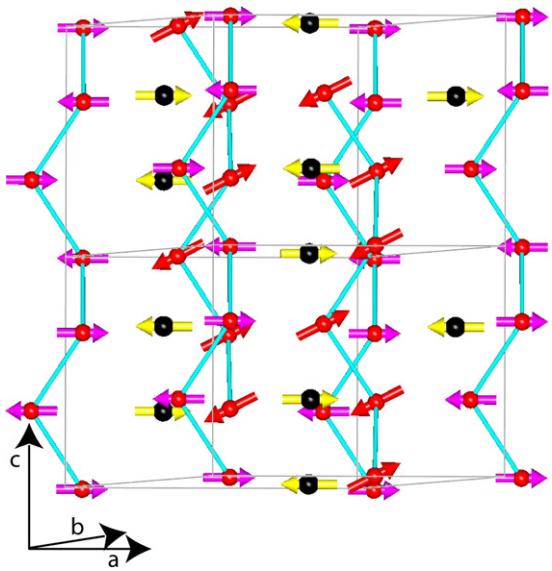

Figure 6. Magnetic structure of $HoFe_3(BO_3)_4$ at 6 K. Fe spins in red (grey, horizontal) (Fe2) or magenta (grey, inclined) (Fe1), Ho spins in yellow (light grey).

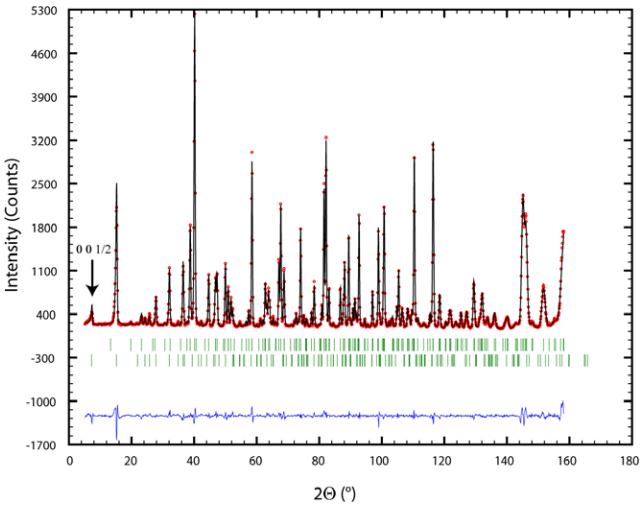

Figure 7. Observed (dots, red), calculated (line, black) and difference pattern of $HoFe_3(BO_3)_4$ at 2 K refined in $P3_121$. The tick marks indicate the calculated position of the nuclear (upper row) and magnetic (lower row) Bragg peaks.

the magnetic structure as found for the Y compound the high resolution data of $HoFe_3(BO_4)_3$ were refined between 5 and 40 K. An attempt to simulate the spectra solely with a magnetic contribution coming from the Fe spins did not succeed and led to the conclusion that already above 5 K both sublattices, the rare earth and the iron one, are magnetically long-range-ordered.

As a further difference from the situation in the Y compound the refinement has to include a spin component in the z direction of the Fe sublattice. The analysis of the data shows that, while there is no noticeable difference between the basal spin components of the two Fe sublattices, the z component is non-zero only for one of the two Fe sublattices. As the refinement cannot make a difference between this z component being on the Fe2 sublattice or on the Fe1 sublattice a physical argument had to be used to decide on the most probable situation: refining a z component on the Fe1 sublattice (comprising 6 Fe spins within the c-direction doubled magnetic unit cell) the total magnetic moment of this site amounts to 5.4 μ_B at 6 K (4.3 μ_B on the Fe2 site), a value clearly too high to be physically reasonable, while when putting the z component on the Fe2 sublattice (comprising 12 Fe spins) the total magnetic moment values amount to 4.8 μ_B for the Fe2 site and 4.2 μ_B on the Fe1 site. Figure 6 shows the magnetic structure of $HoFe_3(BO_3)_4$ below 37 K down to about 5 K.

The magnetic structure adopted by $HoFe_3(BO_3)_4$ below 5 K is very similar to the one found in $TbFe_3(BO_3)_4$ [10]. This magnetic structure had been determined using magnetic symmetry analysis using the program BASIREPS included in the FULLPROF suite of programs [13]. The correct irreducible representation describing the magnetic couplings has two, three and two basis functions for the Fe1, Fe2 and Ho sites. Allowing the coefficients of these basis functions to refine independently it became clear that, similar to the situation of the Tb compound, the coefficients of the basis functions corresponding to a spin component in the z direction had to be coupled for the two different Fe sites. There is no spin component in the x–y-direction present on either of the two Fe sublattices. However, and this represents a difference for the case of the Tb compound, a significant spin component in the x–y direction can be found on the Ho sublattice where the main component is pointing in the z direction. Figure 7 shows the final refinement of the 2 K neutron diffraction data of $HoFe_3(BO_3)_4$.

The intensity of the magnetic Bragg peak at $2\Theta = 7.3°$ corresponding to the 0 0 1/2 peak is solely determined by the presence of this additional spin component in the x–y direction on the Ho sublattice. Figure 8 displays the magnetic structure found below the spin reorientation at 5 K. The x–y component on the Ho sublattice adopts an arrangement where the Ho spins have an angle of 60° to each other, going from one a–b plane to the neighbouring one. This contrasts with the overall

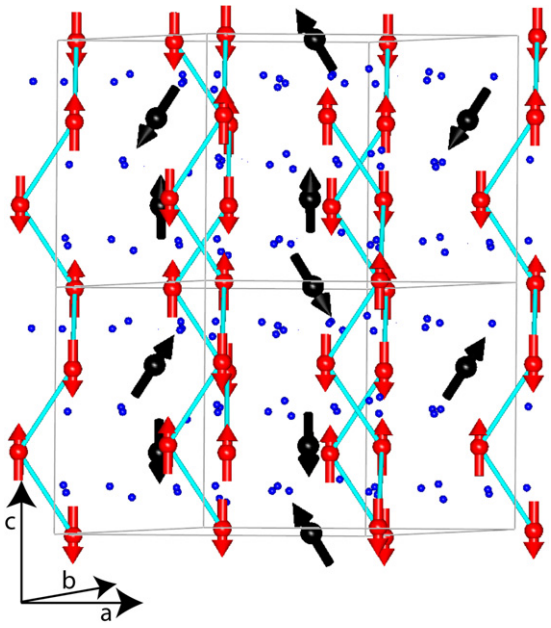

Figure 8. Magnetic structure of $HoFe_3(BO_3)_4$ at 2 K. Fe spins in red (grey) and Ho spins in black. The position of the oxygen atoms is represented by small blue (black) spheres.

simple antiferromagnetic up–down symmetry of the magnetic coupling in the z direction. Comparing figures 6 and 8 one sees that, while it is justified to speak of a simple spin-reorientation process as far as the Fe sublattices are concerned, the spin reorientation of the Ho sublattice involves not only a collective rotation of the Ho spins out of the a–b plane into the c direction but an additional rotation as well perpendicular to either one of the three $a1$, $a2$, $a3$ hexagonal lattice vectors of the basal plane in the four-index Miller Bravais system.

Once the magnetic structures of $HoFe_3(BO_3)_4$ had been determined, the temperature-dependent high resolution data were fitted sequentially. Figure 9 shows the evolution of the individual spin components as a function of temperature.

Several conclusions can be drawn from these plots: the onset of the long-range magnetic order is simultaneous for the Fe and the Ho sublattice. The temperature dependence of the Ho-moment value shows an accelerated increase down to about 10 K (figure 9(c)), the temperature where the x component of the Fe moment reaches its greatest value. This indicates strongly that the Ho moment value increase is governed by the polarization effect of the Fe sublattice, as it is induced by the magnetically ordered surroundings. One has to recall here that, due to the isolated situation of the rare-earth trigonal prisms RO_6, the direct exchange interactions through the f-electrons between neighbouring Ho spins should be very weak. The strong influence of the Fe sublattice on the rare-earth magnetism is responsible as well for the non-Brillouin type behaviour of the temperature dependence of the total iron magnetic moment (figure 9(b)). Present already just below T_N, the z component of the Fe sublattice increases steadily on cooling and gets significant just above T_{SR}. At the spin reorientation the x component turns by 90°, leading to a collinear magnetic structure of the Fe sublattices. This reorientation leads, however, to a reduction of the total magnetic moment on the Fe sites from about 4.8 μ_B at 5 K to 4.4 μ_B at 2 K. This value coincides exactly with the value of the total magnetic moment found in the isostructural Tb compound which sees the same spin orientation of the Fe sublattice. The sequential refinement of the high resolution data permitted the search for subtle structural changes between 40 K and the base temperature in the Ho compound. Surprisingly there are no noticeable changes in any of the interatomic distances or angles. This leads to the conclusion that the structure which hosts the magnetic spins is not influenced by the magnetic order and the magnetic exchange interactions. It is even tempting to propose the opposite: structural details limiting the strength of the exchange interactions force the reduction of the total magnetic moment on the Fe site down to 4.4 μ_B once the spins are oriented in the c direction.

This point of view is supported by the astonishingly small total moment developed on the Ho site of about 5 μ_B which has to be compared to the free ion moment for Ho^{3+} of gJ (μ_B) = 10 μ_B. The temperature-dependent increase of the Ho magnetic moment stops abruptly at the spin-reorientation temperature as if competing magnetic interactions force the magnetic moment values of both sublattices into a 'frozen compromise'. In this context it is evident that the low temperature orientation of the Fe-sublattice moments is determined by the rare-earth magnetism. This follows from the fact that, in the isostructural Y compound, which has nearly identical interatomic distances and angles the orientation is within the basal plane. The increase of the Ho-sublattice magnetization drives the spin reorientation of the Fe sublattice in a parallel direction over the Ho–O–Fe–O–Ho interactions. This mirrors a temperature-dependent competition between the anisotropies of the rare earth and iron sublattices. The orientation of the rare-earth sublattice itself must be determined by its single-ion anisotropy and leads to a low temperature structure as already found for the similar Tb compound [10]. Whereas down to about 5 K the easy-plane type magnetic structure is imposed by the Fe sublattice, below this temperature (confirming the results of [12]) the easy-axis type magnetic structure is imposed by the Ho sublattice as well on the Fe sublattice through the Ho(f)–O–Fe(d) superexchange interactions. The case of $TbFe_3(BO_3)_4$ seems to be special as the strong influence of the Tb sublattice (8.5 μ_B at 2 K) leads already immediately at T_N to a spin orientation along the c direction. The low temperature magnetic moment value in $YFe_3(BO_3)_4$ is, at 3.9 μ_B, significantly lower than in $NdFe_3(BO_3)_4$ [11] with both compounds having the spins of the Fe sublattice oriented within the basal plane. Bond valence calculations using the determined Fe–O distances show that the iron ion is present as Fe^{3+} which should lead to a saturation moment of about 5 μ_B. The low value of the ordered Fe moment may be linked to the presence of the one-dimensional structural element which limits the establishment of a 3D network of interactions. It is tempting to interpret the difference between the magnetic moment values of the Y and Nd compounds in terms of the supporting influence of the Nd-sublattice magnetism lying within the basal plane. However, one has to await further results on other rare-earth

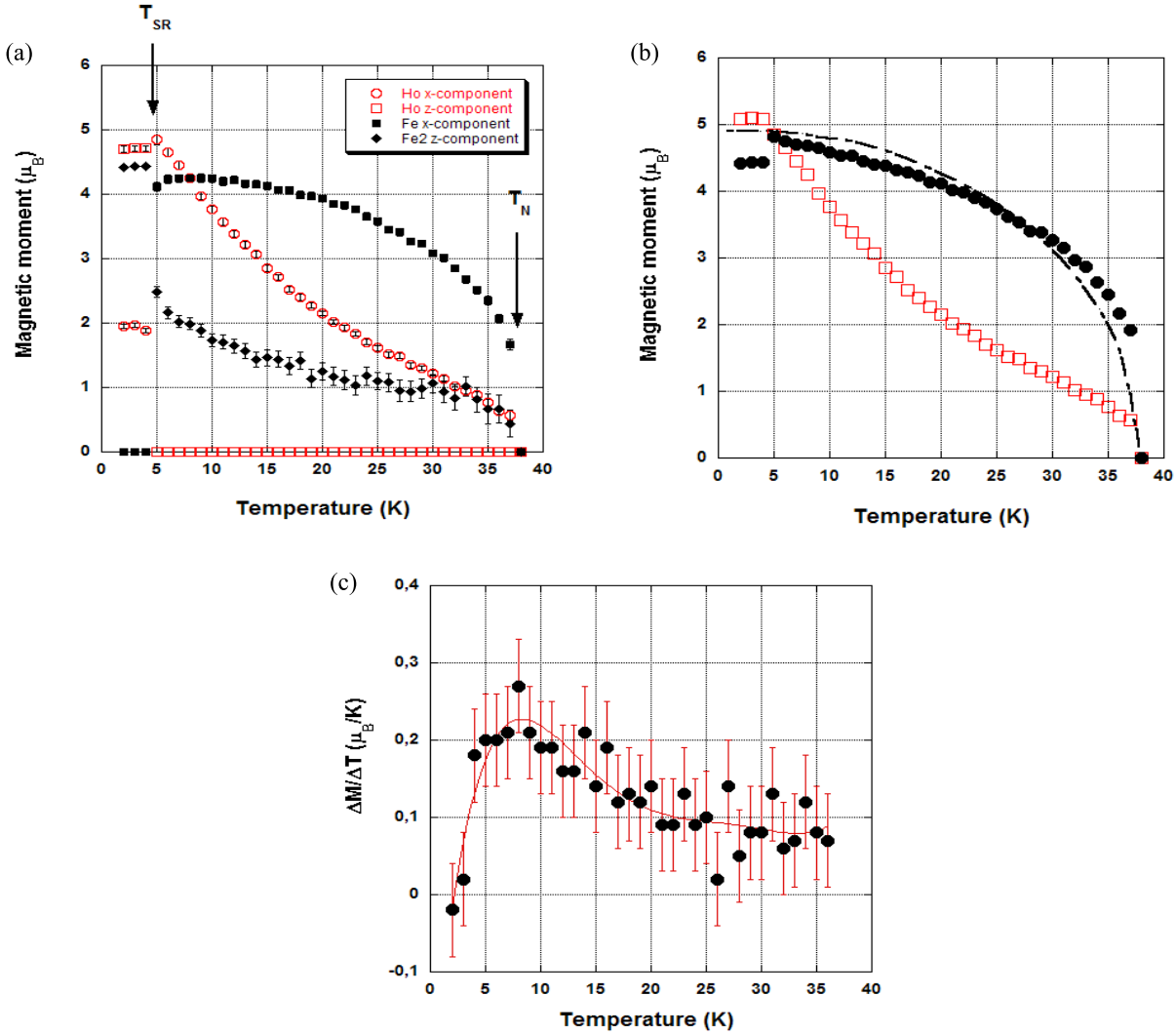

Figure 9. (a) Temperature dependence of the individual magnetic moment components, T_{SR} = spin reorientation temperature. (b) Temperature dependence of the total moments, solid circles = Fe moment, open squares = Ho moment. (c) Temperature dependence of the Ho-moment increase.

ferroborates as the structural differences between the small rare-earth compounds with RE = Y, Ho and Tb and the case of the large Nd can be important concerning the decisive intra and interchain Fe–Fe exchange interactions.

The magnetic structure of $HoFe_3(BO_3)_4$ as determined from neutron diffraction data was confirmed by magnetic measurements. Figure 10 shows the temperature dependences of magnetic susceptibilities measured for $H \parallel c$ and $H \perp c$. At temperatures $T > 100$ K the susceptibilities follow a Curie–Weiss law with the parameters $\theta_{\parallel} = -28$ K, $\theta_{\perp} = -17$ K and $\mu_{\mathrm{eff}\parallel} = 13.60\ \mu_B$, $\mu_{\mathrm{eff}\perp} = 12.69\ \mu_B$ per formula unit. These parameters are effective ones averaged over the rare-earth and iron subsystems. Both susceptibilities $\chi_{\parallel}$ and $\chi_{\perp}$ are very close to each other at temperatures down to about 20 K. The magnetic ordering temperature is feebly visible in the susceptibility curve but the temperature dependence of the difference $(\chi_{\parallel} - \chi_{\perp})$ shows a distinct peculiarity at the Néel temperature $T_N = 38$ K (see figure 10 inset **a**). A sharp reduction of the parallel susceptibility occurring below 5 K is evident in the inset **b** of figure 10 whereas the perpendicular susceptibility remains almost steady.

These peculiarities are caused by the spontaneous spin reorientation at $T_{SR} = 5$ K. A similar spin reorientation from an easy-plane to an easy-axis magnetic structure due to the temperature-dependent competition between the magnetic anisotropies of rare-earth and iron subsystems was observed in $GdFe_3(BO_3)_4$ at $T_{SR} = 10$ K [14, 15]. The spin reorientation in the last compound is accompanied by a sharp reduction of the parallel susceptibility as well [16].

The field dependences of the magnetization of $HoFe_3(BO_3)_4$ for $H \parallel c$ and $H \perp c$ are depicted in figures 11 and 12. A sudden increase in the magnetization for $H \parallel c$ is evident at $T = 2$ K and absent at $T = 5$ K. This is most likely connected to a field-induced spin reorientation of the magnetic moments from the c-axis direction to the basal plane in a critical field of about 0.4 T, reflecting a change in the anisotropy from easy axis to easy plane. A similar behaviour had been found as well in $GdFe_3(BO_3)_4$ [16] where antiferromagnetic resonance

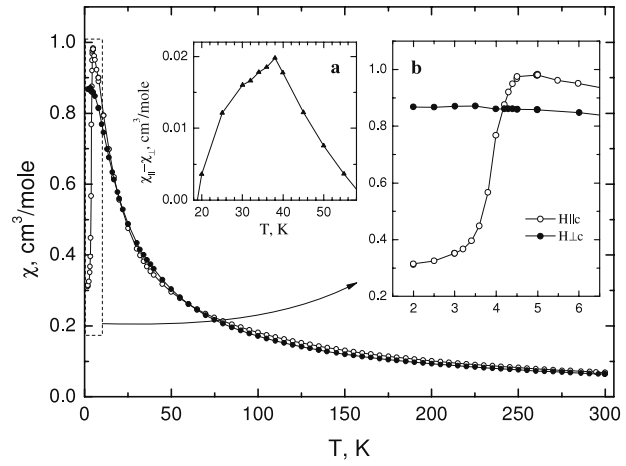

Figure 10. Temperature dependences of magnetic susceptibilities of $HoFe_3(BO_3)_4$ measured in $H \parallel c$ and $H \perp c$ orientations. Insert a—temperature dependence of the difference $(\chi_\parallel - \chi_\perp)$ for $HoFe_3(BO_3)_4$.

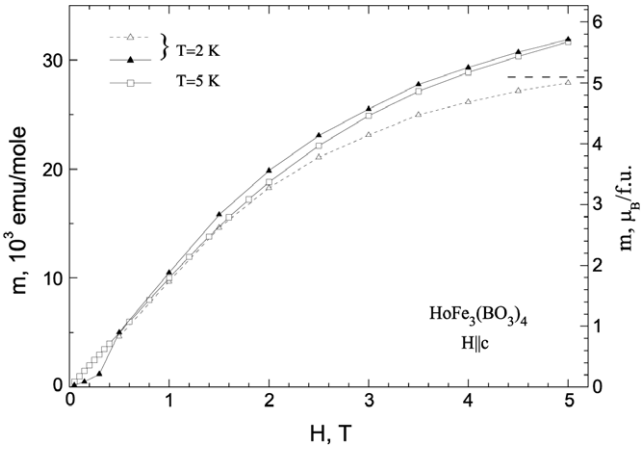

Figure 11. Field dependences of the parallel magnetization and the magnetic moment of Ho^{3+} in $HoFe_3(BO_3)_4$ at 2 and 5 K.

studies [15] had shown that the effect of the external magnetic field does not lead to a spin flop transition but to a change of anisotropy from easy axis to easy plane. The critical field of this transition tends to zero as $T \to T_{SR}$, forming the magnetic phase diagram of $GdFe_3(BO_3)_4$ [14, 15]. In a similar way the critical field tends from 0.4 T at 2 K to zero at $T \to T_{SR} = 5$ K in the Ho compound studied here.

The contribution of the antiferromagnetically ordered Fe^{3+} subsystem to the magnetization at field values larger than the reorientation field depends linearly on the field with $\chi_\perp = 1.4 \times 10^{-4}$ cm^3 g^{-1} [5] and can be subtracted from the total magnetization. The residual part shown by open triangles in figure 11 belongs to the Ho^{3+} ions; its saturation corresponds to the magnetic moment of the Ho^{3+} ion which coincides well with $\mu \approx 5.1\ \mu_B$ obtained from neutron diffraction and marked by a dashed line. For $H \perp c$ the field dependence of magnetization of $HoFe_3(BO_3)_4$ at $T = 2$ K is slightly nonlinear below 1 T as well (see figure 12). This is probably connected to the domain structure arising below T_{SR} in the basal plane of the crystal due to the transversal components of the Ho moment.

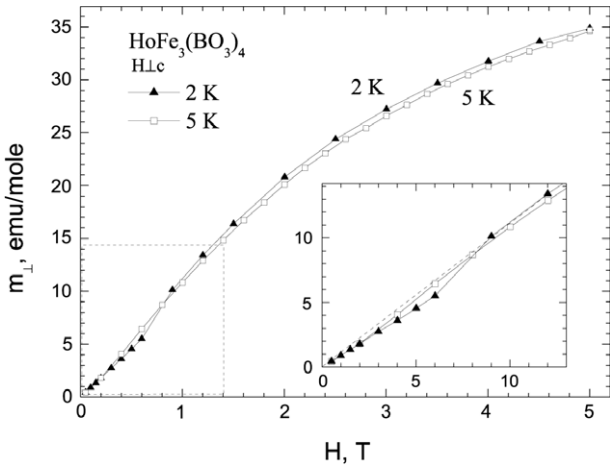

Figure 12. Field dependences of magnetization in $HoFe_3(BO_3)_4$ at 2 and 5 K, $H \perp c$.

4. Summary

Neutron diffraction and magnetization studies of the iron borates $RFe_3(BO_3)_4$ (R = Y, Ho) were carried out as a function of temperature. The presence of the non-magnetic (Y) or the magnetic (Ho) (and Tb [10]) ions allows us to track the mutual influence of the Fe and R sublattices on the long-range magnetic structures evolving depending on the different kinds of rare-earth ion. Due to the similarity of the crystal structures of these compounds it becomes possible to concentrate one's attention on the magnetic behaviour determined either only by the iron sublattice (R = Y) or by the additional influence of the anisotropy of the various rare-earth ions. First of all, we have to conclude the simultaneous increase of the long-range magnetic order for both sublattices (Fe, R = Tb [10], Ho, Nd [11]) with T_N lying in the range from 30 to 40 K, depending on the type of R. This allows us to deduce a strong polarization effect of the Fe sublattice on the rare-earth ions since the R–O–R exchange pathways are absent in these compounds. For the Y compound the magnetic peaks can be indexed with a magnetic propagation vector $\tau = [0\ 0\ 1/2]$ corresponding to a magnetic unit cell doubled in the hexagonal c direction. The easy-plane magnetic structure sees the Fe spins antiferromagnetically coupled in the c direction while being ferromagnetically coupled within the a–b basal plane. There is no sign of a spin-reorientation process; both Fe sublattices behave identically.

In contrast, the Ho compound sees already just below T_N a non-zero component on the Fe2 sublattice along the c axis with Fe1 and Ho spins lying exclusively in the basal plane. The value of the Fe2 component along the c axis increases steadily while decreasing the temperature. A spin reorientation occurs at $T_{SR} = 5$ K where both Fe sublattices orientate parallel to the c direction. The reorientation of the Ho sublattice involves not only a collective rotation of the Ho spins out of the a–b plane into the c direction but an additional rotation perpendicular to either one of the three $a1$, $a2$, $a3$ hexagonal lattice vectors of the basal plane as well.

Taking into account the available data as well for the Tb [10] and the Nd compounds [11] it is possible to

propose that different kinds of magnetic structures are realized, depending on the rare-earth magnetic moment value and anisotropy. Starting from the non-magnetic Y ion the easy-plane configuration of the magnetic moments is determined solely by the magnetic anisotropy of the Fe ions. With increasing rare-earth moment a tendency of the magnetic structure type to change from easy plane to easy axis via easy plane incommensurate for Nd^{3+} ($\mu \sim 2.7\ \mu_B$) [11], non-coplanar with subsequent easy axis $[0, 0, 1/2]$ for Ho^{3+} ($\mu \sim 5\ \mu_B$) and finally pure easy axis $[0, 0, 1/2]$ for Tb^{3+} ($\mu \sim 8.6\ \mu_B$) compound can be stated. It is obvious that these transformations are governed by the temperature-dependent competition between the anisotropies of the rare-earth and iron sublattices. The magnetic measurements confirm the magnetic structure of $HoFe_3(BO_3)_4$ determined from neutron diffraction data. A spin reorientation back from an easy-axis to an easy-plane magnetic structure was found at $T = 2$ K in a magnetic field $H = 0.4$ T parallel to the c axis. Measurements on $PrFe_3(BO_3)_4$ and on the even larger $LaFe_3(BO_3)_4$ are underway or planned in order to broaden the available database on these highly interesting compounds.

Acknowledgment

This work was supported by RFBR, grant no. 06-02-16255.

References

[1] Jaque D 2001 *J. Alloys Compounds* **323/324** 204
[2] Chen X, Luo Z, Romero J J, Sole J G, Huang Y, Jiang A and Tu Ch 2001 *J. Phys.: Condens. Matter* **13** 1171
[3] Kalashnicova A M, Pavlov V V, Pisarev R V, Bezmaternykh L N, Bayer M and Rasing Th 2004 *JETP Lett.* **80** 293
[4] Zvezdin A K, Krotov S S, Kadomtseva A M, Vorob'ev G P, Popov Yu F, Pyatakov A P, Bezmaternykh L N, Kuvardin A V and Popova E N 2005 *JETP Lett.* **81** 272
[5] Zvezdin A K, Vorob'ev G P, Kadomtseva A M, Popov Yu F, Pyatakov A P, Bezmaternykh L N, Kuvardin A V and Popova E N 2006 *JETP Lett.* **83** 509
[6] Leonyuk N I and Leonyuk L I 1995 *Prog. Cryst. Growth Charact. Mater.* **31** 179
[7] Campa J A, Cascales C, Guttierez-Puebla E, Monge M A, Rasines I and Ruiz-Valero C 1997 *Chem. Mater.* **9** 237
[8] Klimin S A, Fausti D, Meetsma A, Bezmaternykh L N, van Loosdrecht P H M and Palstra T T M 2005 *Acta Crystallogr.* B **61** 481
[9] Hinatsu Y, Doi Y, Ito K, Wakeshima M and Alemi A 2003 *J. Solid State Chem.* **172** 438
[10] Ritter C, Balaev A, Vorotynov A, Petrakovskii G, Velikanov D, Temerov V and Gudim I 2007 *J. Phys.: Condens. Matter* **19** 196227
[11] Fischer P, Pomjakushin V, Sheptyakov D, Keller L, Janoschek M, Roessli B, Schefer J, Petrakovskii G, Bezmaternykh L, Temerov V and Velikanov D 2006 *J. Phys.: Condens. Matter* **18** 7975
[12] Stanislavshuk T N, Chukalina E P, Popova M N, Bezmaternykh L N and Gudim I A 2007 *Phys. Lett.* A **368** 408
[13] Rodriguez-Carvajal J 1993 *Physica* B **192** 55
[14] Pankrats A I, Petrakovskii G A, Bezmaternykh L N and Temerov V L 2008 *Phys. Solid State* **50** 79
[15] Pankrats A I, Petrakovskii G A, Bezmaternykh L N and Bayukov O A 2004 *JETP* **99** 766
[16] Balaev A D, Bezmaternykh L N, Gudim I A, Temerov V L, Ovchinnikov S G and Kharlamova S A 2003 *J. Magn. Magn. Mater.* **258/259** 532